



## Observations of a variety of drainage patterns in bamboo foams

To cite this article: V. Carrier *et al* 2008 *EPL* **83** 54005

View the [article online](#) for updates and enhancements.

### You may also like

- [Highly nonparaxial propagation and optical power exchange in uniaxial crystals: Analytical and numerical study](#)  
Chao Yu, Xiancong Lu, Xiaozhong Wang et al.
- [Floquet-Bloch waves in one-dimensional photonic crystals](#)  
G. V. Morozov and D. W. L. Sprung
- [A general model for dislocation contribution to acoustic nonlinearity](#)  
Jianfeng Zhang and Fu-zhen Xuan

# Observations of a variety of drainage patterns in bamboo foams

V. CARRIER, S. HUTZLER<sup>(a)</sup> and D. WEAIRE

*School of Physics, Trinity College Dublin - Dublin 2, Ireland*

received 9 November 2007; accepted in final form 18 July 2008

published online 2 September 2008

PACS 47.54.-r – Fluid dynamics: Pattern selection; pattern formation

PACS 47.20.Ky – Flow instabilities: Nonlinearity, bifurcation, and symmetry breaking

PACS 82.70.Rr – Aerosols and foams

**Abstract** – We have explored the patterns of drainage in a bamboo foam, *i.e.* a foam consisting of an arrangement of parallel soap films with equidistant spacing. We find an intriguing variety of such patterns, both static and dynamic. All involve the formation of drainage channels at the wall of the column, which are variously arranged and in some cases rotating and oscillating.

Copyright © EPLA, 2008

**Introduction.** – One of the simplest systems that can be made from soap bubbles is “bamboo foam” [1–3], in which the bubbles are trapped in a narrow cylindrical tube. They are separated by transverse soap films, at whose perimeter a surface Plateau border, or Gibbs ring, is formed. When this column is placed vertically and additional liquid is introduced at the top, its behaviour is anomalous, in comparison with the drainage properties of bulk foams. If the tube has a radius less than a certain critical value, defined below, the additional liquid accumulates at the top, there being no measurable drainage via the wetting films on the tube wall. This observation [4] is consistent with the classic studies of Bretherton [5]. In the present letter we closely examine what happens for larger tube radii, and report a rich variety of static and dynamic patterns of drainage, of which examples are shown in figs. 1 and 2.

Throughout all of our experiments the bubbles remain arranged in the bamboo structure, with the addition of vertical channels permitting drainage between the horizontal surface Plateau borders. The observed drainage patterns are therefore distinct from those previously reported, which involve structural rearrangements of the bubbles themselves [6,7].

**Experimental arrangement.** – The critical tube radius  $R_c$  for drainage is approximately [4]

$$R_c = 0.92l_0, \quad (1)$$

where  $l_0 = \sqrt{\frac{\sigma}{\rho g}}$ . This is the familiar capillary length of a liquid of density  $\rho$  and surface tension  $\sigma$  under gravity  $g$ .

For typical surfactant solutions  $\sigma$  is of the order of 25 to 30 mN/m. For the 0.3% vol. solution of the commercial detergent Fairy Liquid used in this experiment the value of  $l_0$  is about 1.7 mm.

We used plain glass tubes, 50 cm in length, with radii between 1 and 10 mm. Bubbles were created by blowing nitrogen, saturated with perfluorohexane vapour to prevent coarsening, into the Fairy Liquid solution and then collected in the vertically aligned glass tubes. Care was taken to ensure the accurate vertical alignment of the tube; failure to do this was seen to introduce artifacts. Bubble volumes were in the range from 30 mm<sup>3</sup> to 10<sup>4</sup> mm<sup>3</sup>. In each experiment the ratio of tube to bubble radius was kept in the range between 0.5 and 1.1, thus resulting in the formation of a bamboo structure [8].

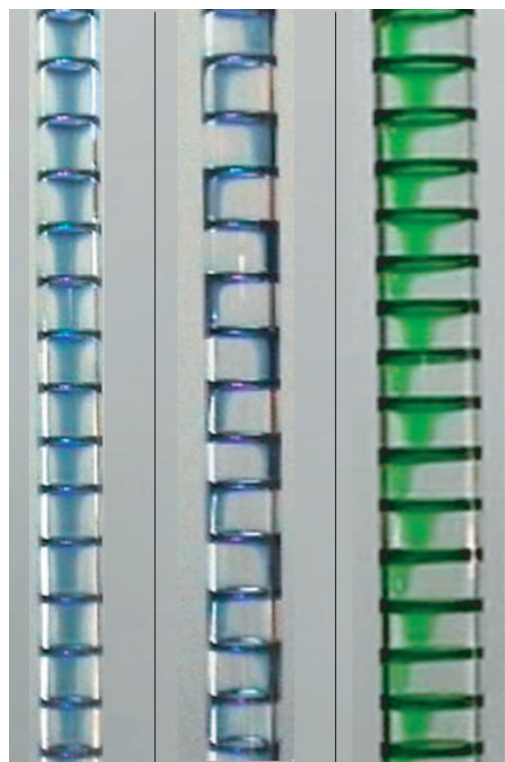
Solution was added at the top of the bamboo foam using a peristaltic pump and a rubber tube which was attached to the side of the glass tube. For the photos and videos that were taken, dyes were added to the solution.

**Ordered drainage patterns.** – In addition to the tube radius  $R$ , the volume rate  $Q$  of addition of liquid is important in determining the type of drainage pattern. These two parameters may be used to define regimes of occurrence of the different patterns, as in fig. 3, in a “phase diagram”. This diagram is based on about 200 individual observations.

*Regime A:* no observed drainage. As previously discussed [4], no drainage is observed in this regime, even after very long times (several days).

*Regime B:* Here there is continuous drainage through vertical channels at the wall of the tube, connecting successive Plateau borders. The channels are fixed in position. They form a static alternating pattern along the tube

<sup>(a)</sup>E-mail: stefan.hutzler@tcd.ie



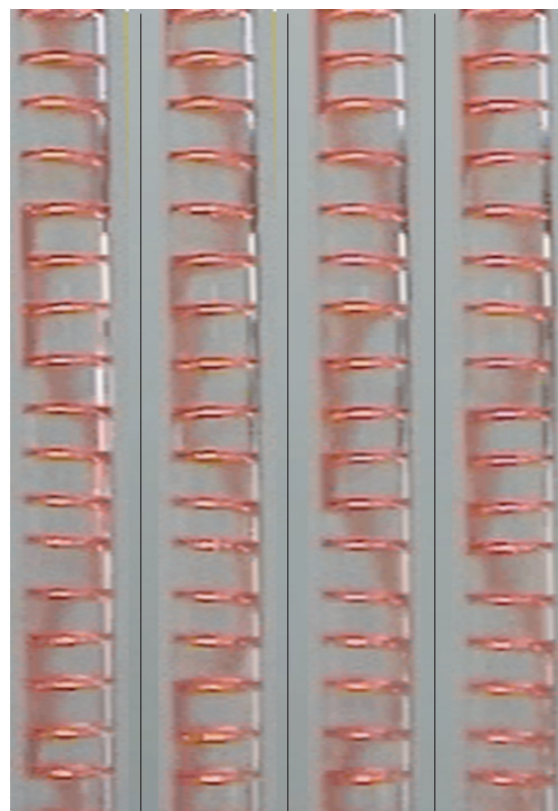
(a) Regime E (b) Regime B (c) Regime B  
(narrow tube) (wide tube)

Fig. 1: Drainage of bamboo foams proceeds through vertical channels (visible as dark vertical stripes) that are formed at the wall of the tube, connecting successive horizontal Plateau borders. For the examples shown here the location of the channels does not change in time. Depending on the flow rate of liquid added at the top, successive channels are either separated by a constant spacing around the tube diameter (*regime B*), or all aligned with the feeding point (*regime E*).

axis. For tubes with radii equal or less than the capillary length, successive channels are situated at opposite sides of the tube, see fig. 1(b). For larger tube radii we find that the spacing between two channels (measured around the circumference of the tube) is about three times the capillary length, *i.e.* approximately 5 mm. This is independent of flow rate, tube radius and the spacing between consecutive films. In this case the channels are thus located on the same side of the tube, as is shown in fig. 1(c).

*Regime C*: In this regime the pattern of channels is no longer static. Downwards propagating oscillations occur (see fig. 2), with wavelengths greatly exceeding the spacing of the transverse films and periods ranging between thirty seconds and three minutes.

*Regime D*: Another phase is observed between regime B and C which corresponds to a chaotic motion of the channels. This incorporates oscillations, rotations inside the tube in either direction, and also periods where no motion occurs.



Regime C

0 seconds 4 seconds 8 seconds 12 seconds  
time →

Fig. 2: For an appropriate choice of flow rate and tube radius, consistent with *regime C* of fig. 3, the channels connecting successive horizontal Plateau borders are not fixed but oscillate in a propagative wave. The amplitude of the oscillation is approximately one quarter of the perimeter of the tube, *i.e.* the channels stay on the same side of the tube.

*Regime E*: Finally for flow rates above 50 mm<sup>3</sup>/s, the channel is a static straight line aligned with the feeding point (see fig. 1(a)).

**The oscillatory regime.** – From fig. 3 we can see that regime C is roughly defined by flow rates  $Q$  between 5 and 50 mm<sup>3</sup>/s and tube radius  $R$  exceeding about 2.3 times the capillary length. From visual observations we find that the amplitude of the wave is almost always close to one quarter of the perimeter of the tube, independent of the values of  $R$ ,  $L$  and  $Q$ . The wavelength  $\lambda$  is proportional to the spacing  $L$  between consecutive films. Its dependence on the flow rate is shown in fig. 4. For small values of  $Q$  the ratio  $\lambda/L$  varies strongly and appears not to be well defined, while for higher values of  $Q$  it is independent of  $Q$ . We found that this  $Q$ -independent value of  $\lambda/L$  generally increases with the tube radius, ranging from  $\lambda/L \simeq 4$  for  $R/l_0 = 2.9$  to  $\lambda/L \simeq 16$  for  $R/l_0 = 4.5$ . However, occasionally we found that for the same value of  $R/l_0$  the

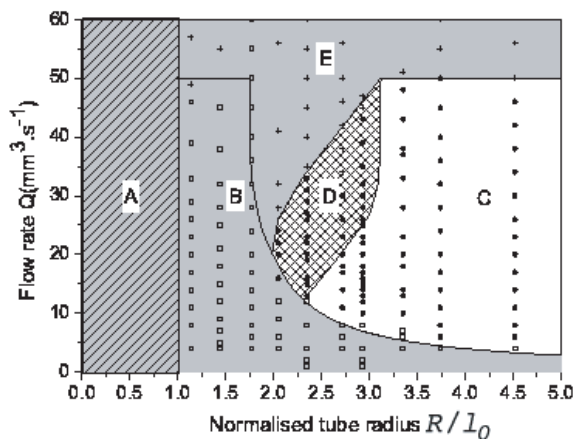


Fig. 3: “Phase diagram” for the flow dynamics of bamboo foams as a function of flow rate  $Q$  and tube radius  $R$  (normalised by the capillary length  $l_0 = 1.69$  mm). The symbols correspond to experimental observations and the lines and shaded regions are guides to the eye. The hatched region corresponds to the *no-flow* regime A, the grey regime represents the *static flow* patterns of regime B (open squares) and E (crosses). Regime C is characterised by *oscillatory motion* of the channels. Region D with cross-hatched shading corresponds to *chaotic motion* of the channels.

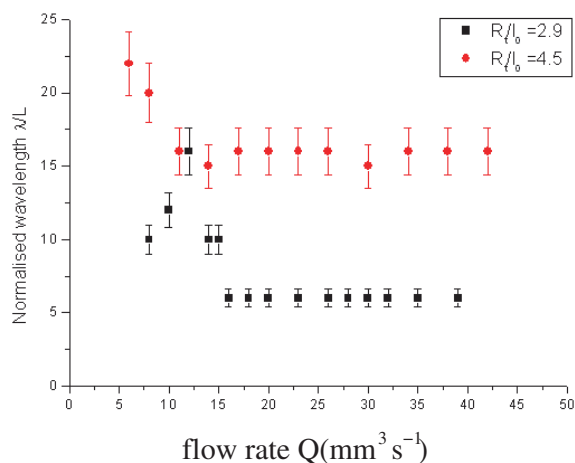


Fig. 4: Regime C: for values of flow rate  $Q$  exceeding  $15 \text{ mm}^3/\text{s}$  the wavelength  $\lambda$  (normalised by the spacing  $L$  of the soap films) is independent of  $Q$ . The data shown is for a ratio of tube radius  $R$  to capillary length  $l_0$  of 2.9 and 4.5, respectively.

wavelength can take on integer multiples of the minimal measured wavelength  $\lambda/L \simeq 4$ , *i.e.* there is evidence of harmonics.

Values for the frequency  $\omega$  of the wave as a function of flow rate  $Q$  were obtained using a stopwatch. We find that  $\omega$  increases linearly with  $Q$ , with a slope that is inversely proportional to the bubble spacing  $L$ . This is shown in fig. 5 where the plot of  $\omega L$  as a function of flow rate collapses data for three different values of  $L$  onto one straight line, thus establishing  $\omega = cQ/L$ , where  $c$  is a proportionality constant.

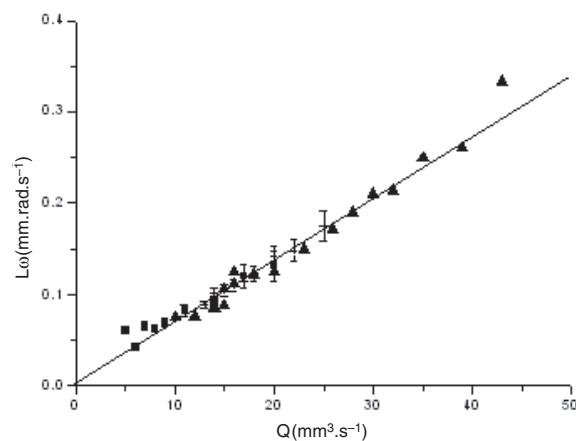


Fig. 5: Regime C: the frequency of the oscillation increases linearly with flow rate and is inversely proportional to the spacing  $L$  of the soap films, resulting in  $L\omega \propto Q$ . The data shown is for  $L = 5.4$  mm (squares),  $L = 9.5$  mm (crosses) and  $L = 12$  mm (triangles). Here the tube radius was kept constant,  $R/l_0 = 2.9$ .

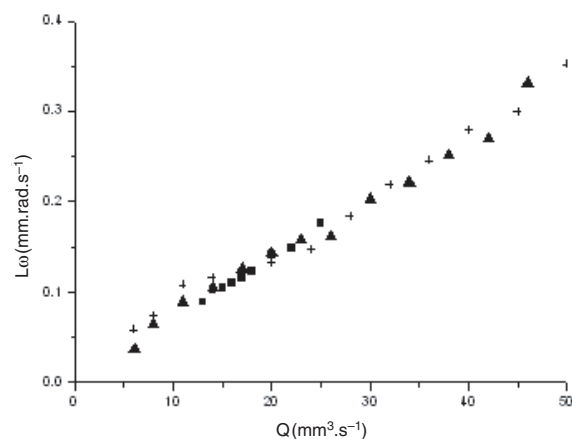


Fig. 6: Regime C:  $L\omega$  is proportional to  $Q$ , independent of the tube radius. The data shown is for  $R/l_0 = 2.9$  (squares),  $R/l_0 = 3.7$  (crosses) and  $R/l_0 = 4.5$  (triangles). Here  $L \simeq 9.5$  mm is kept constant for all the data.

Figure 6 shows the variation of  $\omega L$  with  $Q$  for bamboo foams in tubes of three different radii. The value of  $c$  is thus independent of the tube radius,  $c = 6.87 \times 10^3 \text{ mm}^{-2}$  as obtained from least-square fits of our data.

**Discussion.** – The forces responsible for the observed flow regimes are not immediately obvious. The Reynolds number  $Re$ , defined as  $Re = \frac{Q}{\nu L}$ , where  $\nu$  is the kinematic viscosity (we take the value for water,  $\nu = 1.0 \text{ mm}^2 \text{ s}^{-1}$ ) and  $L$  the distance between two films ( $L \approx 1$  cm), is of the order of unity for the range of values of  $Q$  studied. This implies that both viscous and inertial forces may play a role in the observed drainage patterns.

Their explanation probably requires an answer to the following question: how can a channel coexist with a wetting film? The Laplace pressure inside the channel is higher than in the wetting film, which requires a balancing force for stabilisation. By analogy with the “tears of wine” and marginal regeneration this could be related to Marangoni forces, but more experiments and theory (see, for example, the numerical work on flow instabilities in draining thin liquid films in [9]) are clearly needed to clarify this. Also, while our experiments with other surfactants show similar drainage patterns, the details of the phase diagram differ, indicating a strong dependence on the physico-chemical characteristics of the surfactants. In particular when using the surfactant SDBS we have observed a different regime, where all channels rotate together around the tube with a constant velocity. Also, regimes C and D are shifted to higher tube radii, and the rotation regime appears at normalised tube radii in the range  $2 < R/l_0 < 3$ .

This observed list of phenomena is very interesting in comparison with other one-dimensional systems which show non-linear dynamics. Examples are the printer’s instability [10–12], the fluid fountain [13–19] and the meandering flow of a rivulet of surfactant solution descending under gravity between two narrowly spaced glass plates [20]. The drainage patterns in bamboo foams appear to have some similarities with these systems, *e.g.* the parity-breaking instability. However, while in these systems the length scale is an intrinsic constant parameter, in the bamboo foam it is a tunable parameter (via flow rate or tube radius). This opens the door to numerous experimental and theoretical studies of the behaviour of such systems with composite length scales. Yet another important feature in the observed oscillations of the vertical channels in our experiments is still puzzling: contrarily to most 1d non-linear dynamical systems, wavelength doubling is almost never observed, and quite surprisingly, stable  $Q$ -independent large wavelengths occur (up to  $22L$  for large tube radii); also this remains to be understood.

While we are not in a position to propose a definitive theory of the observed drainage patterns, some preliminary ideas are included in the appendix. The basic model that we suggest successfully mimics the main features of the system. However, the phase diagram built from the model still does not quantitatively look like the experimental one, which is not surprising, given the extreme and speculative nature of the model. However, it does suggest that the ingredients of a full and well-founded theory need not be very complex.

\*\*\*

Research is supported by ESA/ESTEC (14914/02/NL/SH (AO 99-108), 14308/00/NL/SH (AO 99-031)), Science Foundation Ireland (05/RFP/PHY0016) (VC), and the European Science Foundation COST (European Science Foundation) Action P21 “Physics of Droplets”.

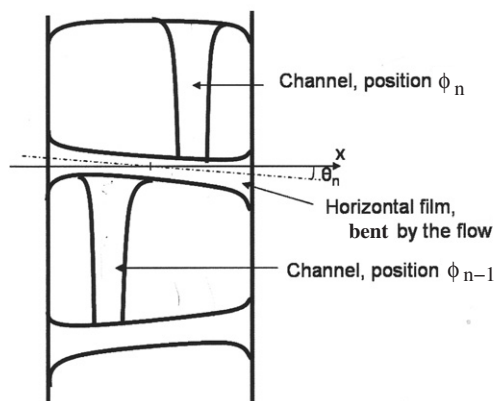


Fig. 7: Sketch of the geometry in our model. The horizontal films are bent at an angle  $\Theta_n$  to the horizontal due to flow. The vertical channels are in contact with the cylinder walls, and are located at angles  $\Phi_n$ .

#### APPENDIX

**Phenomenological theory.** – We take for granted the existence of the vertical channels (at the wall of the tube) that connect the horizontal Plateau borders, each of which has a position represented by an angle  $\Phi_n$ , where channel  $n$  connects Plateau border  $n$  and  $n + 1$ . Each Plateau border is deflected from the horizontal by an angle  $\Theta_n$ , as sketched in fig. 7. The analogies mentioned in the previous section Discussion suggest the following interpretation: successive channels are pulled apart by centrifugal forces due to flow inertia, as in rivulet instability [20], and this is opposed by the time-dependent bending of the film, due to flow inertia again. A simple model can be constructed to illustrate this idea, based on the two coupled variables  $\Phi_n$  and  $\Theta_n$ , the displacement of the channels and the tilt of the borders, respectively.

The equation of evolution for  $\Theta_n$  is written as a balance between three forces or moments,

$$f_l R^2 \frac{d\Theta_n}{dt} = \rho v Q R \sin(\Phi_n - \Phi_{n-1}) - C \sigma R^2 \Theta_n. \quad (\text{A.1})$$

The term on the left-hand side is due to viscous forces, where  $f_l$  is the coefficient of the drag of the film on the plate (assumed for simplicity to be linear) and  $R$  is the tube radius. The first term of the right-hand side is the moment due to the change of momentum at the channel/border junction ( $v$  is the velocity of the flow and  $Q$  is the flow rate). Consideration of the special cases  $\Phi_n = \Phi_{n-1}$  and  $\Phi_n = \Phi_{n-1} + \pi$  suggests the sinusoidal form used here. The motion is opposed by the restoring force (second term on the right-hand side) due to surface tension  $\sigma$ , where  $C$  is a constant.

Assuming Poiseuille flow through the channels one obtains

$$v = \left(\frac{\rho g}{2\eta}\right)^{1/2} \left(\frac{Q}{K_1}\right)^{1/2}, \quad (\text{A.2})$$

where  $\eta$  is the liquid viscosity and  $K_1$  is a numerical factor accounting for the flow in the channel [21–23].

The equation of evolution for  $\Phi_n$  is written as a balance of three forces,

$$f_2 L_c \frac{d\Phi_n}{dt} = \rho v Q [\text{Sgn}(\Phi_n - \Phi_{n-1}) + \text{Sgn}(\Phi_n - \Phi_{n+1})] - B a_{pb} \Theta_n. \quad (\text{A.3})$$

The left-hand side represents the viscous forces, proportional to the length of the channel,  $L_c = L - l_{hf}$ , where  $l_{hf}$  stands for the height of the horizontal film and is approximately equal to  $2l_0$ ;  $f_2$  is a coefficient of friction for the channel on the plate. The first term on the right-hand side corresponds to the horizontal component of the rate of change of momentum of the descending fluid.  $\text{Sgn}$  is the sign function, defined by  $\text{Sgn}(x) = \frac{x}{|x|}$ . The last term represents the attraction between successive channels due to film bending, which we set proportional to the product of the cross-section of the channel  $a_{pb} = Q/v$  and  $\Theta_n$ ,  $B$  is a constant. As the channel is in a tube,  $\Phi_n$  is defined modulo  $2\pi$  in the range  $[-\pi, +\pi]$ .

Using eq. (A.2), the two eqs. (A.1) and (A.3) reduce to

$$f_1' \frac{d\Theta_n}{dt} = \frac{Q^{3/2}}{R} \sin(\Phi_n - \Phi_{n-1}) - C' \Theta_n \quad (\text{A.4})$$

and

$$f_2' L_c \frac{d\Phi_n}{dt} = Q^{3/2} [\text{Sgn}(\Phi_n - \Phi_{n-1}) + \text{Sgn}(\Phi_n - \Phi_{n+1})] - B' Q^{1/2} \Phi_n. \quad (\text{A.5})$$

A numerical solution of this set of equations shows that this model has four states similar to the experimental ones: at low values of  $Q$  the vertical channels are located opposite to each other for small  $R$ , and they alternate at high  $R$ ; at high values of  $Q$ , the channels rotate for small values of  $R$ , and they oscillate at high  $R$ , with a chaotic regime between the rotation and oscillation attractors, where the channels either rotate or oscillate.

In the alternate state the separation between successive channels slightly decreases with  $Q$ , roughly as  $Q^{-1/2}$ , and increases with surface tension. At intermediate flow rates propagative oscillations develop, with an amplitude equaling a quarter of the tube perimeter, independent of  $Q$ . The frequency varies as  $\omega \propto \frac{Q}{\sqrt{L-2l_0}}$ . The wavelength decreases with  $Q$  and tends towards  $2L$ , which is two bubbles, in a wavelength doubling or “optical” mode [16–19]. The rotation state corresponds to a rotation of

all the channels with a frequency  $\omega \propto \frac{Q^{3/2}}{L-2l_0}$ , each channel rotates in opposite direction to the previous channel, again showing wavelength doubling.

Furthermore, the experimentally observed aligned state at high  $Q$  can be modelled by adding a destabilising term  $\Theta_n^2$  to the right-hand side of eq. (A.5).

## REFERENCES

- [1] WEAIRE D. and HUTZLER S., *The Physics of Foams* (Clarendon Press, Oxford) 1999.
- [2] WEAIRE D., HUTZLER S. and PITTET N., *Forma*, **7** (1992) 259.
- [3] PITTET N., BOLTENHAGEN P., RIVIER N. and WEAIRE D., *Europhys. Lett.*, **35** (1996) 547.
- [4] CARRIER V., HUTZLER S. and WEAIRE D., *Colloids Surf. A: Physicochem. Eng. Aspects*, **309** (2007) 13.
- [5] BRETHERTON F. P., *J. Fluid Mech.*, **10** (1961) 166.
- [6] BOLTENHAGEN P., PITTET N. and RIVIER N., *Europhys. Lett.*, **43** (1998) 690.
- [7] REINELT D., BOLTENHAGEN P. and RIVIER N., *Eur. Phys. J. E*, **4** (2001) 299.
- [8] PITTET N., RIVIER N. and WEAIRE D., *Forma*, **10** (1995) 65.
- [9] BRAUN R. J., SNOW S. A. and NAIRE S., *J. Eng. Math.*, **43** (2002) 281.
- [10] RABAUD M., MICHALLAND S. and COUDER Y., *Phys. Rev. Lett.*, **64** (1990) 184.
- [11] CUMMINS H. Z., FOURTUNE L. and RABAUD M., *Phys. Rev. E*, **47** (1993) 1727.
- [12] PAN L. and DE BRUYN J. R., *Phys. Rev. E*, **49** (1994) 483.
- [13] LE GRAND-PITEIRA N., DAERR A. and LIMAT L., *Phys. Rev. Lett.*, **96** (2006) 254503.
- [14] GIORGIUTTI F., BLETTON A., LIMAT L. and WESFREID J. E., *Phys. Rev. Lett.*, **74** (1995) 538.
- [15] GIORGIUTTI F. and LIMAT L., *Physica D*, **103** (1997) 590.
- [16] GIORGIUTTI F., LIMAT L. and WESFREID J. E., *Phys. Rev. E*, **57** (1998) 2843.
- [17] COUNILLON C., DAUDET L., PODGORSKI T. and LIMAT L., *Phys. Rev. Lett.*, **80** (1998) 2117.
- [18] BRUNET B., FLESSELLES J.-M. and LIMAT L., *Eur. Phys. J. B*, **35** (2003) 525.
- [19] BRUNET P. and LIMAT L., *Phys. Rev. E*, **70** (2004) 046207.
- [20] DRENCKHAN W., GATZ S. and WEAIRE D., *Phys. Fluids*, **16** (2004) 31115.
- [21] LEONARD R. A. and LEMLICH R., *AIChE J.*, **11** (1965) 18.
- [22] DESAI D. and KUMAR R., *Chem. Eng. Sci.*, **37** (1982) 1361.
- [23] KOEHLER S., HILGENFELDT S. and STONE H. A., *J. Colloid Interface Sci.*, **276** (2004) 420.